Human leucocyte antigen G (HLA-G) and its murine homologue Qa-2 protect from pregnancy loss

Stefanie Dietz
Tuebingen University Children's Hospital
Julian Schwarz
Tuebingen University Children's Hospital
Ana Velic
University of Tuebingen
Irene Gonzalez Menendez
Institute of Pathology and Comprehensive Cancer Center, Eberhard Karls Universität Tübingen
Leticia Quintanilla-Martinez
University of Tuebingen
Nicolas Casadei
Eberhard Karls University Tübingen https://orcid.org/0000-0003-2209-0580
Alexander Marmé
Practice for Gynecology
Christian Poets
Tuebingen University Children's Hospital
Christian Gille
Tuebingen University Children's Hospital
Natascha Köstlin-Gille (natascha.koestlin@med.uni-tuebingen.de)
Tuebingen University Children's Hospital https://orcid.org/0000-0003-3718-5507

Article

Keywords: innate immune cells, infertility, reproductive disorders

Posted Date: June 16th, 2021

DOI: https://doi.org/10.21203/rs.3.rs-554398/v1

Abstract

During pregnancy, the maternal immune system has to balance tightly between protection against pathogens and tolerance towards a semi-allogeneic organism. Dysfunction of this immune adaptation can lead to severe complications such as pregnancy loss, preeclampsia or fetal growth restriction. The MHC-Ib molecule HLA-G is well known to mediate immunological tolerance. However, no *in-vivo* studies have yet demonstrated a beneficial role of HLA-G for pregnancy success. Myeloid derived suppressor cells (MDSC) are suppressively acting immune cells accumulating during pregnancy and mediating maternal-fetal tolerance. Here, we analyzed the impact of Qa-2, the murine homologue to HLA-G, on pregnancy outcome *in vivo*. We demonstrate that lack of Qa-2 led to intrauterine growth restriction and increased abortion rates especially in late pregnancy accompanied by changes in uterine gene expression, altered spiral artery remodeling and protein aggregation in trophoblast cells indicating a preeclampsia-like phenotype. Furthermore, lack of Qa-2 caused decreased accumulation of MDSC and impaired MDSC function. Lastly, we show that application of sHLA-G reduced abortion rates in Qa-2 deficient mice by inducing MDSC. Our results highlight the importance of an interaction between HLA-G and MDSC for pregnancy success and the therapeutic potential of HLA-G for the treatment of immunological pregnancy complications.

Introduction

Premature termination of pregnancy either by abortion or by preterm delivery is the most important pregnancy complication. At least 25%, but probably up to 50% of women suffer miscarriage and about 10% of infants are delivered preterm[1,2]. Besides chromosomal or anatomic anomalies and endocrinological disorders, immunological factors play an important role in abortion pathogenesis and preterm delivery. During pregnancy, there is a close contact between maternal immune cells and fetal cells. Thus, the maternal immune system has to balance tightly between protection against pathogens and tolerance towards the semi-allogeneic fetus. Dysfunction of the immune adaptation to pregnancy can lead to severe complications such as pregnancy loss, preeclampsia, preterm birth or fetal growth restriction. The mechanisms facilitating maternal-fetal tolerance are only incompletely understood and therapeutic options are limited.

The major histocompatibility class Ib (MHC Ib) molecule human leucocyte antigen G (HLA-G) is a non-classical MHC I molecule with low allelic variation and a restricted peptide repertoire[3]. Under physiological conditions, HLA-G is mainly expressed by trophoblast cells at the maternal-fetal interface and can be secreted in a soluble form (soluble HLA-G, sHLAG) to the circulation[3]. *In vitro* studies show that HLA-G shapes the maternal immune system towards tolerance by induction of a tolerogenic phenotype of antigen-presenting cells (APCs)[4] as well as inhibition of T-cell activity[5] and natural killer cell (NK-cell) cytotoxicity[6]. During an uncomplicated pregnancy, levels of sHLA-G first increase and then decrease until the third trimester. Undetectable sHLA-G levels or variation in the course of sHLA-G levels

seem to be related with gestational complications such as spontaneous abortion and preeclampsia[7]. As yet, however, no *in-vivo* studies exist that demonstrate a beneficial role of HLA-G for pregnancy success.

Qa-2 has been described as the murine homolog to HLA-G[8]. Mice not expressing the Qa-2 antigen ($Qa2^-$) have smaller litters and a shorter duration of gestation than Qa-2 expressing animals[9]. On the fetal side, presence of Qa-2 seems to protect from rejection[9]. Mechanisms mediating the protective role of Qa-2 during reproduction are only incompletely understood.

Myeloid derived suppressor cells (MDSC) are myeloid cells with various immune suppressive properties. They mainly consist of two subtypes named granulocytic MDSC (GR-MDSC) with phenotypic characteristics of neutrophils and monocytic MDSC (MO-MDSC) with phenotypic similarities to monocytes. In mice, GR-MDSC are defined as $CD11b^+/Ly6G^+/Ly6C^{lo}$ and MO-MDSC as $CD11b^+/Ly6G^-/Ly6C^{hi}$ cells[10]. Primarily, MDSC accumulation has been described under tumor conditions where they suppress immune responses against tumor cells, thereby leading to disease progression[11]. Later, MDSC have been shown to accumulate under various other pathologies like infection, trauma, autoimmune disease, obesity and transplantation[12]. In recent years, however, there is increasing evidence that MDSC also play a physiological role during pregnancy by modulating maternal immune responses and protecting the fetus from rejection[13-17]. Accumulation and activation of MDSC are driven by various factors[10]. Recently, we demonstrated, that HLA-G induced and activated GR-MDSC *in-vitro*[18].

In the present study, we investigated the *in-vivo* role of HLA-G for pregnancy success by using mice not expressing the Qa-2 antigen (Qa-2 negative, $Qa2^-$, B6.K1) and showed that lack of Qa-2 leads to intrauterine growth restriction and increased abortion rates with profound changes in uterine gene expression profile and uterine spiral arteries and trophoblasts, indicating a preeclampsia-like phenotype. Immunological adaptation to pregnancy was imbalanced with missing MDSC accumulation and impaired MDSC function. By application of sHLA-G to $Qa\text{-}2^-$ mice we could reduce their increased abortion rate, highlighting its therapeutic potential for treatment of immunological pregnancy complications.

Results

Qa-2 deficiency in mice leads to adverse pregnancy outcome in late pregnancy

To evaluate the impact of Qa-2 on pregnancy outcome, we analyzed mice lacking the Qa-2 antigen ($Qa\text{-}2^-$, B6.K1). Compared to WT mice, we found significantly smaller litter sizes in $Qa\text{-}2^-$ animals (Figure 1A). At mid-pregnancy (E10.5), $Qa\text{-}2^-$ mice had similar numbers of intact fetuses compared to WT mice (Supplementary Figure 1A) and slightly increased abortion rates (Supplementary Figure 1B+C). At E18.5, however, lack of Qa-2 led to an abortion rate of 17% in comparison to 5% in WT animals (Figure 1B+C). Furthermore $Qa\text{-}2^-$ fetuses weighed significantly less than WT fetuses (Figure 1D+E).

Qa-2 deficiency leads to changes in the uterine gene expression profile

Since many adaptation processes to pregnancy take place in the uterus, we next performed transcriptome analyses of whole uterine lysates. Of 610 differentially regulated genes, 380 were upregulated in WT uteri and 230 were upregulated in
Qa-2$^-$ uteri. Network analysis using the STRING database[19] showed enrichment of genes encoding for proteins involved in various specific biological processes in WT animals (Figure 2A), among which “immune system processes”, “nervous system development” and “circulatory system development” were the processes with most genes detected. Among immunological processes upregulated in WT uteri, especially cytokine/chemokine signaling, myeloid cell differentiation, apoptosis regulation, leucocyte migration and lymphocyte activation were involved (Figure 2B). Genes upregulated in Qa-2$^-$ animals showed no clustering to any biological process.

Qa-2 deficiency leads to altered spiral artery remodeling and altered trophoblast morphology

Since spiral artery remodeling is a crucial step in maternal adaptation to pregnancy, and transcriptome analyses revealed profound differences in uterine expression of genes involved in vasculogenesis between WT and Qa-2$^-$ animals, we next analyzed spiral arteries in E10.5 pregnant WT and Qa-2$^-$ animals. In Qa-2$^-$ animals, we found large areas within the decidua with unorganized trophoblast distribution, while in WT animals, trophoblasts proper organized around the vessels, pointing to an abnormal trophoblast-migration in Qa-2$^-$ mice (Figure 3A). In addition, spiral arteries of Qa-2$^-$ animals had thicker vessel walls than that of WT mice, while luminal areas did not differ (Figure 3 B-D).

Furthermore, we found changes in placenta histology between E18.5 old WT and Qa-2$^-$ fetuses; placentas from both genotypes showed similar cross-section areas (Figure 3E); however, while placentas from WT animals showed long and thin villi with proper morphology, placentas from Qa-2$^-$ animals showed irregular and short villi and abnormal vacuolization of the trophoblast and numerous eosinophilic aggregates. On a scale of 0 (no aggregates) to 2 (prominent aggregates), the phenotype of WT placentas was 0.2 ± 0.4 while that of Qa-2$^-$ placentas was 1.4 ± 1.0 (Figure 3F+G and Supplementary Figure 2). These aggregates were still present in PAS-diastase staining, indicating that they were not glycogen (Figure 3H). Proteome analyses of whole placenta lysates from WT and Qa-2$^-$ animals showed strong enrichment in proteins involved in protein metabolism processes (GO:0019538), especially in translation (GO:0006412), proteolysis (GO:0006508), phosphorylation (GO:0016310) and dephosphorylation (GO:0006470) (Supplementary Figure 3) in Qa-2$^-$ placentas (184 of 655 proteins only detected in Qa-2$^-$), suggesting dysfunctional protein storage in trophoblasts of these animals.

Systemic and uterine accumulation of MDSC during pregnancy is abrogated in Qa-2$^-$ mice

Since it is known that HLA-G plays an important role in immune regulation during pregnancy[20] and transcriptome analyses showed upregulation of genes involved in immune system processes, we analyzed immune cell populations in spleen and uterus of Qa-2$^-$ and WT mice. We observed a strong increase in total splenic MDSC, as well as in splenic GR-MDSC and MO-MDSC between non-pregnant WT

animals and WT animals at E18.5. In Qa-2$^-$ animals however, there was only a marginal increase in total splenic MDSC at E18.5, while neither GR-MDSC nor MO-MDSC numbers increased (Figure 4A-D). Correspondingly, we found strongly increased numbers of uterine MDSC in WT animals at E18.5 in comparison to non-pregnant controls, but not in Qa-2$^-$ animals (Figure 4E+F). Conversely, in Qa-2$^-$ mice we found an increase in splenic T-cells and a decrease in splenic B-cells upon pregnancy, while splenic T-cell and B-cell numbers in WT mice remained unchanged. In WT mice, but not Qa-2$^-$ mice, splenic NK-cells and splenic monocytes increased (Supplementary Figure 4A-D). Changes in uterine lymphocyte populations during pregnancy did not differ between WT and Qa2$^-$ animals (Supplementary Figure 3E-G), while uterine monocytes decreased in WT animals, but not Qa2$^-$ animals. No differences were observed in placental immune cell composition between Qa-2$^-$ and WT placentas (Supplementary Figure 5A-E).

Qa2 deficiency leads to changes in T-cell subpopulations during pregnancy and to a decreased capacity of MDSC to induce T_{regs}

We further investigated whether there were any differences in T-cell subpopulations between pregnant WT and Qa-2$^-$ animals at E18.5. Gating strategy for T-cell subpopulations is depicted in Figure 5A, and phenotyping strategy is depicted in Figure 5B. No differences were found in percentages of T-helper cells and cytotoxic T-cells between WT and Qa-2$^-$ animals (Figure 5C+G). Qa-2$^-$ animals had higher numbers of effector memory $CD4^+$ and $CD8^+$ T-cells and lower numbers of central memory $CD4^+$ and naïve $CD8^+$ T-cells (Figure 5D-F and H-J). Furthermore, Qa-2$^-$ animals had significantly less T_{reg}- and more Th17-cells, while there were no differences in numbers of Th1- and Th2-cells (Figure 5K-P). Decreased numbers of T_{regs} in Qa-2$^-$ animals were confirmed by intracellular staining of FoxP3 (Figure 3Q+R).

Induction of T_{regs} is a main feature of MDSC[21,22]. We thus analyzed the capacity of Qa-2$^-$ MDSC to induce T_{regs} in comparison to that of WT MDSC *in vitro*. T_{regs} were induced by both, WT and Qa-2$^-$ MDSC, although to a lower extend in the latter (Figure 6A+B). Capacity of Qa-2$^-$ MDSC to inhibit T-cell proliferation was also reduced in comparison to WT MDSC, but the difference did not reach significance (Figure 6C+D).

Expression of Qa-2 on MDSC is regulated by estrogen via HIF-1α

As Qa-2 seemed to be relevant for MDSC function, we next asked how Qa-2$^-$ expression may be regulated. Flow cytometric analyses of Qa-2 expression on MDSC and T-cells revealed that in non-pregnant WT mice between 10% and 60% of MDSC and all T-cells expressed Qa-2; pregnancy induced the expression of Qa-2 both on MDSC and T-cells (Figure 7A-C). The same effect could be observed for HLA-G-expression on human MDSC (Figure 7D+E). To get hints on a potential hormonal regulation of Qa-2 expression on immune cells, we analyzed blood of female mice during the menstrual cycle and found increased Qa-2 expression on MDSC during proestrus and estrus, the phases with higher estrogen levels[23], than during metestrus and diestrus (Figure 7F+G). To further evaluate the effect of estrogen on Qa-2 expression on MDSC, we next stimulated spleen cells of WT mice with

increasing concentrations of estrogen and showed that Qa-2 expression on MDSC increased upon estrogen stimulation in a concentration dependent manner, while Qa-2 expression on T-cells did not change (Figure 7H-J). Recent data showed that expression of HLA-G on tumor cells can be regulated by the transcription factor hypoxia-inducible factor 1α (HIF-1α)[24,25] and that HIF-1α regulates MDSC function during murine pregnancy[15]. We thus assumed that expression of Qa-2 on MDSC may be regulated by HIF-1α and stimulated spleen cells of WT mice with classic (anoxia) and alternative (*Escherichia coli*, *E. coli*) stimuli of HIF-1α. We showed that both anoxia and *E. coli s*timulation led to an increased expression of Qa-2 on MDSC (Figure 8A-C), but not on T-cells (Figure 8D+E). Correspondingly, MDSC isolated from pregnant mice with targeted deletion of HIF-1α in myeloid cells (HIF-KO) expressed lower levels of Qa-2 than MDSC isolated from WT mice (Figure 8F). Stimulation of myeloid HIF-KO MDSC with estrogen did not result in an upregulation of Qa-2 expression (Figure 8G). Taken together, our results show that expression of Qa-2 on MDSC is at least partly regulated by estrogen via HIF-1α.

Application of sHLA-G improves pregnancy outcome

Lastly, we asked whether we could restore pregnancy success in Qa-2$^-$ animals by application of sHLA-G. Pregnant Qa-2$^-$ mice received either 1µg/g bodyweight sHLA-G or PBS at E10.5 and E14.5. Application of sHLA-G led to a pronounced reduction in the abortion rate of Qa-2$^-$ animals (Figure 9A), accompanied by a partial restoration of normal trophoblast morphology (Figure 9B). Furthermore, it marginally increased splenic MDSC, but strongly increased uterine MDSC (Figure 9C-E). Simultaneous depletion of MDSC with sHLA-G application reversed the pregnancy-protective effect of sHLA-G (Figure 9F). To confirm the beneficial effect of sHLA-G on pregnancy outcome in another model, we treated abortion-prone DBA/2J-mated CBA/J mice with sHLA-G or PBS at E0.5, E3.5, E6.5 and E9.5. Also in this model, application of sHLA-G significantly reduced abortion rates (Figure 9G+H).

Discussion

Our data show that Qa-2 is relevant for pregnancy success and protects from late pregnancy loss by regulating immune adaptation to pregnancy in terms of promoting MDSC accumulation and modulating T-cell homeostasis. We further show that expression of Qa-2 on MDSC is relevant for their functionality and regulated by estrogen via HIF-1α. Lastly, we show that application of sHLA-G to abortion-prone Qa-2$^-$ mice decreases abortion rates via induction of MDSC.

It has been shown for a long time that HLA-G is highly expressed during pregnancy especially by trophoblast cells[3] mediating various immune-modulatory effects *in vitro*[4-6]*.* Furthermore, alterations of HLA-G expression during pregnancy are associated with adverse pregnancy outcome[26-28]. Until now, however, no studies provided *in vivo* evidence that HLA-G indeed is needed for a successful pregnancy. We used Qa-2 deficient mice to evaluate the *in vivo* role of Qa-2/HLA-G for pregnancy outcome and found smaller litter sizes and growth restriction in surviving fetuses in Qa-2$^-$ animals in comparison to WT animals. These results confirm previous studies also describing smaller litters and smaller offspring in

Qa-2$^-$ animals[9,29]. Interestingly, expression of Qa-2 on the fetal side was found to be advantageous for survival, leading to a higher embryonic cleavage rate[9,30]. We now show increased rates of pregnancy loss in Qa-2$^-$ animals especially during late pregnancy accompanied by profound changes in maternal adaptation to pregnancy in comparison to WT mice, demonstrating that Qa-2 not only plays a local role in fetal tissue but is also systemically needed in the maternal organism to facilitate a successful pregnancy.

In transcriptome analyses of whole uteri, we found prominent differences between Qa-2$^-$ and WT animals in transcripts regulating angiogenesis. Corresponding to that, we found altered spiral artery morphology in Qa-2$^-$ in comparison to WT animals. Remodeling of uterine spiral arteries is one of the critical steps in maternal adaptation to pregnancy as it permits normal placental perfusion and fetal growth and development[31]. Inadequate spiral artery remodeling results in placental hypoxia and may lead to development of preeclampsia and fetal growth restriction[32]. In Qa-2$^-$ placentas, we observed profound changes in trophoblast morphology in comparison to WT placentas with cytoplasmic storage of eosinophilic aggregates and enrichment of proteins involved in protein metabolism. Interestingly, it has been shown that during preeclampsia, misfolded proteins accumulate in urine, serum and placenta similar to the protein accumulation observed in neurodegenerative disorders like Alzheimer´s disease[33-35]. Our findings of dysregulation of uterine vasculogenesis, fetal growth restriction, late abortions and pathological protein storage in placenta may suggest the development of a preeclampsia-like phenotype in Qa-2$^-$ mice. This assumption is supported by recent data showing that injection of an anti-Qa-2 antibody led to preeclampsia symptoms in mice that could be abrogated by simultaneous injection of recombinant VEGF[36].

Furthermore, we found significant differences in immunological adaptation to pregnancy between WT and Qa-2$^-$ animals. Both, systemically and locally in the uterus, we observed a strong increase in MDSC in WT but not in Qa-2$^-$ mice. The accumulation of MDSC and its relevance for successful pregnancy has been described previously in different mouse models (reviewed in[37]). However, all these studies focused on early- to mid-gestation, showing that depletion of MDSC in early gestation or genetically determined decreased MDSC accumulation at E10.5 led to complete gestation failure[16] or increased abortion rates[15,17]. Our present results now illustrate that MDSC accumulation also seems to be relevant for pregnancy success in later stages of pregnancy. Contrarily to our results, Ostrand-Rosenberg et al. showed that depletion of MDSC at E8.5 did not lead to adverse pregnancy outcome[16]. However, since antibody-mediated MDSC depletion has to be repeated every three days[38], one injection at E8.5 may be insufficient to examine the role of MDSC until the second half of pregnancy. In correspondence to the increased accumulation of MDSC in uteri of WT mice we observed an upregulation of genes involved in myeloid differentiation and leucocyte migration and chemotaxis in transcriptome analyses of WT whole uterine lysates in comparison to Qa-2$^-$ animals. Furthermore, we previously showed that sHLA-G *in-vitro* led to a quantitative and functional induction of MDSC[18]. We thus assume that a combination of direct and indirect effects of Qa-2 attract MDSC to the pregnant uterus *in-vivo*.

Decreased MDSC accumulation in pregnant Qa-2$^-$ mice was accompanied by an increase in splenic T-cells – an effect that may be associated with miscarriage[39]. Differences in T-cell subpopulations between pregnant WT and Qa-2$^-$ animals mainly concerned effector memory T-cells, T_{regs} and Th17 cells. The CD44$^+$/CD62L$^-$ effector memory CD4$^+$ and CD8$^+$ T-cell subsets were increased in pregnant Qa-2$^-$ mice, while naïve CD8$^+$ and central memory CD4$^+$ T-cells were decreased. This points towards a higher activation status of T-cells in Qa-2$^-$ mice. A recent study showed that effector/activated T-cells led to adverse pregnancy outcome, i.e. preterm birth[40]. Furthermore, patients with preeclampsia downregulate CD62L on T-cells[41]. Since the main effector function of MDSC is an inhibition of T-cell activation, one could hypothesize that increased activation of T-cells in Qa-2$^-$ animals results from a decreased MDSC influence. However, contrary to our results, MDSC downregulate CD62L on T-cells[16,42]. As Qa-2 is also highly expressed on T-cells, the lack of Qa-2 itself may lead to differences in T-cell activation between WT and Qa-2$^-$ mice overlapping the effect of MDSC.

Balance between Th1 and Th2 cells did not differ between WT and Qa-2$^-$ animals, while T_{regs} decreased and Th17 cells increased in pregnant Qa-2$^-$ in comparison to pregnant WT mice, which is similar to findings from normal pregnancies, but the opposite to what is found in patients with recurrent pregnancy loss and preeclampsia[43]. Studies in mice showed that expansion of T_{regs} was relevant for healthy pregnancy and that adoptive transfer of T_{regs} protected from abortions[44,45]. A crosstalk between T_{regs} and MDSC has been described extensively under tumor conditions (reviewed in[46]). Kang et al. described an induction of T_{regs} by MDSC via production of TGFβ *in-vivo* during pregnancy[47], while we showed *in-vitro* that fetal human MDSC as well as exosomes released by MDSC from pregnant women were able to induce T_{regs}[22,48]. We now demonstrate that induction of T_{regs} by MDSC was reduced in absence of Qa-2 on MDSC. This is in line with two studies showing an induction of T_{regs} by mesenchymal stem cells (MSCs) via HLA-G[49]. T_{reg} induction by MDSC may explain the decreased numbers of T_{regs} in pregnant Qa-2$^-$ mice.

Due to the observed functional differences between WT and Qa-2$^-$ MDSC, we asked whether Qa-2 expression on MDSC may be upregulated during pregnancy. We found that MDSC isolated from pregnant individuals (mice and women) expressed higher levels of Qa-2, respectively HLA-G, than MDSC from non-pregnant individuals and that Qa-2 expression on MDSC, but not on T-cells, could be stimulated by estrogen. Immunomodulatory effects of estrogens have been repeatedly described, e.g. an expansion of T_{regs} and a modulation of Th-cell cytokine expression[50,51]. Furthermore, it could be shown that estrogen mediates expansion and functional activation of MDSC[52,53]. However, upregulation of Qa-2 expression on MDSC by estrogen is a yet unknown mechanism. We further show that the effect of estrogen on Qa-2 expression on MDSC was mediated through HIF-1α. This is in line with results from other groups showing that estrogen can activate HIF-1α[54] and that activation of HIF-1α stimulated HLA-G-expression in cancer cells[24,25]. We found that expression of HIF-1α was relevant for MDSC accumulation and function during pregnancy and that targeted deletion of HIF-1α in myeloid cells (myeloid HIF-KO) led to pregnancy failure

in terms of abortions[15]. Our new results suggest that an impaired expression of Qa-2 on MDSC may at least partially be responsible for the adverse pregnancy outcome in myeloid HIF-KO mice.

Lastly, we aimed to investigate the therapeutic effect of sHLA-G on pregnancy outcome and found that application of sHLA-G reduced the abortion rate in Qa-2$^-$ animals, restored placental morphology and induced uterine MDSC accumulation. Simultaneous antibody-mediated depletion of MDSC nullified the protective effect of sHLA-G. Previous studies in mice showed protective effects of HLA-G on transplant rejection[55,56] and collagen-induced arthritis[57]; furthermore, sHLA-G was shown to allow tumor evasion from immunosurveillance[58,59], with some of these effects being mediated by an expansion of MDSC[58-60]. These results together with those reported now suggest that a mutual support of HLA-G and MDSC helps to protect allografts from immune rejection and that this interaction is helpful whenever tolerance is needed to survive (pregnancy, organ transplantation), but detrimental in case of tumor growth.

One limitation of our study is that we used a syngeneic mating model. Since allo-antigens play an important role for immunological pregnancy complications and especially for preeclampsia it may be worth to investigate allogeneic pregnancy. However, in our case, allogeneic mating would have led to expression of Qa-2 by the fetuses making it impossible to investigate the effect of a total lack of Qa-2. Another limitation is that HLA-G is not endogenously expressed in mice. Thus, we used mice lacking Qa-2, the only homologue-candidate for HLA-G yet known, for analyzing its impact on pregnancy outcome. However, although HLA-G is a human MHC I molecule, it binds to the murine paired immunoglobulin-like inhibitory receptor (PIR-B) and mediates tolerogenic effects in mice[61] making it possible to analyze its effects *in-vivo*.

In conclusion, we here describe the impact of Qa-2 on immune adaptation during pregnancy, providing evidence that Qa-2 may prevent the development of preeclampsia and showing *in-vivo* that application of sHLA-G improves pregnancy outcome. These results give reason to hope that synthetic sHLA-G may find a place in the prevention of immunological pregnancy complications like abortions and preeclampsia.

Methods

Study approval

All experiments were approved by the local ethics committee of Tuebingen University (682/2016BO1) for human studies or the regional council Tuebingen (K05/19M, K09/19M, K09/18G, K02/19G, K05/20G and K08/20G) for animal studies.

Mice

B6.K1 (B6.Cg-H2^{b3}/FlaCmwJ, Qa-2$^-$), HIF-1a^{flox} (B6.129-Hif1a^{tm3Rsjo}/J) mice and LysMcre (B6.129P2-*Lyz2*$^{tm1(cre)Ifo}$/J) mice were obtained from The Jackson Laboratory (Bar Harbour, Maine, USA). C57BL/6J (WT) mice, CBA/J and DBA/2J mice were obtained from Charles River (Sulzfeld, Germany). HIF-1a^{flox} mice and LysMcre mice were crossed to get animals with deletion of HIF-1a in myeloid cells (HIF-

1a^{flox}/LysMcre, HIF-KO). All animals were maintained under pathogen-free conditions in the research animal facility of Tuebingen University, Tuebingen, Germany. All experimental animal procedures were conducted according to German federal and state regulations.

Syngeneic matings of Qa-2$^-$, HIF-KO and WT mice and allogeneic matings of CBA/J females with DBA/2J males were set up at 8-12 weeks of age. Gestational ages were determined by visualizing of the presence of a vaginal plug (E0.5 = embryonic day).

Abortion rates were determined by visual inspection of fetal-placental units and defined as ratio of resorbing units to the total number of implantation sites. Resorbing units were either dark, small and necrotic or pale, small and without visible fetus inside the amniotic cavity.

Fetal weight was determined by weighing of E18.5 fetuses immediately after removal from the amniotic cavity.

sHLA-G application and MDSC-depletion

Biotinylated HLA-G1 monomers bound to the peptide KGPPAALTL were kindly provided by Jianhong Cao, Fred Hutchinson Cancer Research Center, Seattle, USA. HLA-G1 tetramers were produced by binding to streptavidin (Biolegend, San Diego, USA).

To test the effect of sHLA-G on pregnancy outcome in Qa2$^-$ mice, pregnant mice were injected intravenously at E10.5 and E14.5 with 1 µg/g body weight HLA-G1 tetramers in 100 µl PBS or with 100 µl PBS alone (control).

For depletion of MDSC, pregnant Qa-2$^-$ mice were injected intravenously at E10.5 and E14.5 with 250µg/mouse Ly6G-antibody (BioXCell, Lebanon, USA) in 100µl dilution buffer (BioXCell) simultaneously with the HLA-G application.

To test the effect of sHLA-G on pregnancy outcome in abortion-prone DBA/2J-mated CBA/J mice, plug-positive mice were injected intravenously with 1 µg/g body weight sHLA-G tetramers in 100 µl PBS or with PBS alone (control) at E0.5, E3.5, E6.5 and E9.5.

Determination of mouse estrous cycle

For identification of the mouse estrous cycle stage, female C57BL/6J mice were anesthetized with 1.5% isoflurane (CP-Pharma, Burgdorf, Germany). Blood was obtained by puncture of the retroorbital vein plexus or the tail vein and vaginal swabs were collected according to an established protocol[23]. A cotton tipped swab (Applimed, Châtel-Saint-Denis, Switzerland) wetted with room-temperature physiological saline was inserted vaginally, gently turned, and then removed. The procedure was repeated twice for four consecutive days with 28 days in between.

The vaginal cells were transferred to a glass slide by rolling the swab over the slide. The slide was air dried, stained with hematoxylin-eosin (HE, Merck GmbH, Darmstadt, Germany) and viewed at 10x magnification under bright field illumination. The cycle stage was determined based on the presence or absence of leucocytes, cornified epithelial cells and nucleated epithelial cells according to[23].

Patients

The local ethics committee approved this study (682/2016BO1) and all women gave written informed consent. From August to October 2019 peripheral blood from pregnant women (aged 18-43 years) was collected during routine blood sampling. Patients suffering from severe pregnancy complications (severe infection, preterm rupture of membranes, preterm labour, preeclampsia/eclampsia), chronic diseases (autoimmune diseases, malignancies, chronic infections) or receiving immune-suppressive therapy were excluded.

Mouse tissue collection and single cell preparations

Non-pregnant and pregnant mice at gestational age E10.5 or E18.5 were euthanized by CO_2 inhalation. Blood (0.5-1 ml) was collected immediately after death by intracardial puncture and placed into EDTA-tubes. Blood plasma was collected after centrifugation of whole blood at 400 rpm. Red blood cells were removed from whole blood by ammonium chloride lysis. Spleens were removed and tissue was pushed through a 100 mm filter (Greiner bio-one, Frickenhausen, Germany) using a syringe plunger. Red blood cells of the spleen were also removed by ammonium chloride lysis and the resulting cell suspension was again passed through a 40 mm filter (Greiner bio-one, Frickenhausen, Germany). Uterine horns were removed in toto. Fetuses and the fetal part of the placenta were dissected from uteri; blood vessels were removed. Uteri were placed into PBS, cut into ~1 mm pieces and pushed through a 40 mm filter. Placentas were pushed through a 100 µm filter using a syringe plunger. Red blood cells were removed by ammonium chloride lysis and the resulting cell suspension was then passed again through a 40 µm filter. All cell suspensions were then adjusted to 1-4x10^6 cells/ml in PBS or medium.

Cell Isolation and Culture

Human peripheral blood mononuclear cells (PBMC) were prepared from EDTA blood samples by Ficoll density gradient centrifugation (lymphocyte separation medium, Biochrom, Berlin, Germany).

To isolate GR-MDSC from murine splenocytes, cells were labeled with Gr-1 Biotin-Antibody and isolated over Streptavidin microbeads followed by a second isolation step using Ly6G Biotin-Antibody and Anti-Biotin microbeads (modified protocol of MDSC Isolation Kit mouse, Miltenyi, Bergisch-Gladbach, Germany). Purity of GR-MDSC after separation was >90%, as determined by flow cytometry.

For isolation of $CD4^+$ T-cells from murine splenocytes, cells were labeled with T-cell Biotin-Antibody Cocktail followed by two consecutive Anti-Biotin magnetic bead separation steps (Miltenyi) according to

the manufacturer´s instructions. Purity of $CD4^+$ T-cells after separation was >90%, as determined by flow cytometry.

In-vitro generation of murine MDSC was performed according to previously established protocols[15,62]. For *in-vitro* generation of MDSC, non-pregnant WT and Qa-2^- mice were euthanized and femora and tibia removed. Bone marrow was collected by flushing the bones with PBS using a syringe and a 25G needle. Bone marrow cells were then washed twice, adjusted to $5x10^5$ cells/ml and cultured for 72 h at 37°C in Dulbecco´s modified eagle medium (DMEM, Thermo Fisher Scientific, Waltham, USA), supplemented with 10 % fetal calf serum (FCS, Biochrom, Berlin, Germany) and 1% penicillin/streptomycin (P/S, Biochrom, Berlin, Germany) supplemented with 100 ng/ml recombinant murine granulocyte colony-stimulating factor (G-CSF, Peprotech, Hamburg, Germany) and 12,5 ng/ml recombinant murine granulocyte-macrophage colony-stimulating factor (GM-CSF, Peprotech, Hamburg, Germany). After 72 h of culture, non-adherent cells were removed and adherent MDSC were detached using 0.5% trypsin/EDTA (Biochrom, Berlin, Germany) and a cell scraper. Purity of Gr-1^+/$CD11b^+$ MDSC was >90%, as determined by flow cytometry.

For induction of T_{regs} by MDSC, *in-vitro* generated MDSC from WT and Qa-2^- mice were co-cultured with freshly isolated murine $CD4^+$ T-cells at a ratio of 2:1 (500 000 T-cells and 250 000 MDSC) in RPMI 1640 with 10% FCS and 1% P/S in 24-well plates at 37°C and 5% CO_2. After 3 days of culture, cells were harvested and intracellular Foxp3 staining was performed. $CD4^+$ T-cells cultured without MDSC served as control.

For analysis of the effect of anoxia, bacterial stimulation or stimulation with estrogen on Qa-2 expression on MDSC, splenocytes from pregnant WT animals or pregnant HIF-KO animals at E10.5 were isolated and cultured overnight in DMEM with 10% FCS and 1% P/S in 24-well plates at 37°C and 5% CO_2. The next day, cells were stimulated for four hours either with anoxia by placing them into a hermetically sealed chamber with anaerobic gas generating sachets (Anaerogen 2.5l, Thermo Fisher Scientific, Waltham, USA), with *E. coli* at a MOI of 1:50, or with estrogen at concentrations of 1 nM, 10 nM and 100 nM (Merck GmbH, Darmstadt, Germany). After four hours, cells were harvested and extracellular staining was performed.

Bacterial culture

E. coli DH5α, an encapsulated K12 laboratory strain was grown in Lennox-Lysogeny-Broth (LB)-medium (Invitrogen, Carlsbad, USA) until early logarithmic growth, resuspended in phosphate buffered saline (PBS, Biochrom, Berlin, Germany) and used immediately

T-cell suppression assay

Freshly isolated $CD4^+$ splenocytes were stained with carboxyfluorescein-succinimidyl ester (CFSE, Invitrogen, Carlsbad, USA) according to the manufacturer´s instructions. Cells were suspended in RPMI

1640 media containing 1% P/S and 10% FCS. CFSE-labelled $CD4^+$ T-cells ($2x10^5$) suspended in 100 ml media were stimulated with $2x10^5$ mouse T-Activator CD3/CD28 Dynabeads (Thermo Fisher Scientific, Waltham, USA) and 50 ng recombinant murine Interleukin-2 (rmIL-2, R&D Systems, Minneapolis, USA) under addition of ß-Mercaptoethanol (Merck, Darmstadt, Germany) at a concentration of 50mM. MDSC isolated from spleens of pregnant WT and $Qa\text{-}2^-$ animals at E10.5 also suspended in RPMI 1640 containing 1% P/S and 10% FCS were added in different ratios (1:2, 1:4 and 1:8). After 3 days of culture, $CD4^+$ T-cell proliferation was determined by flow cytometry using the CFSE dye dilution. Proliferation index, defined as the ratio of $CD4^+$ T-cell proliferation after addition of MDSC and $CD4^+$ T-cell proliferation without MDSC, was determined. $CD4^+$ T-cell proliferation without MDSC was set to a fixed value of 1.

Flow cytometry

Human GR-MDSC were characterized as $CD66b^+/CD14^-/HLA\text{-}DR^{low/-}$ cells, according to previously established protocols for characterization of human MDSC[14]. Antibodies used for extracellular staining of human cells were
anti-CD66b-FITC (clone G10F, concentration 1 µl/$1x10^5$ cells), anti-HLA-G-PE (clone MEM-G/9, concentration 3µl/$1x10^5$ cells), anti-HLA-DR-PerCP-Cy5.5 (clone REA805, concentration 0.1 µl/$1x10^5$ cells) and CD14-APC (clone MφP9, concentration 1 µl/$1x10^5$ cells) (purchased from BD biosciences, Heidelberg, Germany (CD66b and CD14), Miltenyi (HLA-DR) and Exbio, Vestec, Czech Republic (HLA-G)).

For extracellular staining of mouse cells, freshly isolated cells were washed in FACS buffer and fluorescent-conjugated extracellular antibodies were added. Antibodies were purchased from BD Biosciences (CD3 FITC (145-2C11), CD3 PE (17A2), CD4 APC (RM4-5), CD8a APC-H7 (53-6.7), CD8 PE (53-6.7), CD11b Alexa (M1/70), CD19 PE (1D3), CD25 BB515 (PC61), CD44 BB700 (IM7), CD45 BV510 (30-F11), CD45 PerCp (30-F11), CD62L BV421 (MEL-14), CD183 BB700 (CXCR3-173), CD196 BV421 (CCR6), FSV700 Alexa Fluor700, NK1.1 APC (PK136), Gr-1 FITC (RB6-8C5), Gr-1 PerCp (RB6-8C5), Ly-6C FITC (AL-21), Ly-6G PE (1A8)) and Miltenyi (Qa2 PE (REA523)).

For immune cell quantification, cells were pre-gated to CD45. Among $CD45^+$ cells, cell types were identified as follows: T-cells $CD3^+$, T-Helper cells $CD3^+/CD4^+$, cytotoxic T-cells $CD3^+/CD8^+$, B-cells $CD3^-/CD19^+$, NK-cells $CD3^-/NK1.1^+$, MDSC $CD11b^+/Gr\text{-}1^+$, MO-MDSC $CD11b^+/Ly6C^+/Ly6G^-$, GR-MDSC $CD11b^+/Ly6C^{low}/Ly6G^+$ and monocytes $CD11b^+/Gr\text{-}1^-$.

For quantification of T-cell subsets cells were pre-gated to CD45, CD3 and CD4 or CD8. Among $CD45^+/CD3^+/CD4^+$ cells, cell types were identified as follows: naïve T-helper cells $CD44^-/CD62L^+$, effector memory T-helper cells $CD44^+/CD62L^-$, central memory T-helper cells $CD44^+/CD62L^+$, T-helper 1 cells $CXCR3^+/CCR6^-$, T-helper 2 cells $CXCR3^-/CCR6^-$, T-helper 17 cells $CXCR3^-/CCR6^+$, Treg $CD25^+$. Among $CD45^+/CD3^+/CD8^+$ cells, cell types were identified as follows: naïve cytotoxic T-cells $CD44^-/CD62L^+$, effector memory cytotoxic T-cells $CD44^+/CD62L^-$, central memory cytotoxic T-cells $CD44^+/CD62L^+$.

For intracellular staining of Foxp3 cells were extracellular stained with CD4 and CD25 for 30 minutes at 4°C and then incubated in Foxp3 Fixation/Permeabilization working solution (Thermo Fisher Scientific, Waltham, USA) for 60 minutes at room temperature and protected from light. Cells were washed in 1x Permeabilization buffer (Thermo Fisher Scientific) and stained with Foxp3 antibody in 1x permeabilization buffer for 30 minutes at room temperature.

Data acquisition was performed with a FACScalibur flow cytometer or LSR II flow cytometer (BD Bioscience) and analyzed via FlowJo V10 (FlowJo, LLC, Ashland, Oregon, USA).

RNA isolation and transcriptome analyses

For transcriptome analyses of whole uterine lysates, uteri of pregnant WT and Qa-2$^-$ mice at E18.5 were collected, snap-frozen in liquid nitrogen and stored at -80°C until RNA isolation. For RNA isolation, frozen tissue (20-30 mg) was shredded using micro pestles (Sigma Aldrich, St.Louis, USA) and liquid nitrogen to obtain powder. RLT buffer was added and the solution was centrifuged at 8000 rcf. RNA isolation was then performed using the RNeasy Mini Kit (Qiagen, Hilden, Germany).

RNA quality was determined by measuring 260/280 and 230/260 absorbance ratio on a spectrophotometer (Nanodrop ND-1000; Peqlab, Erlangen, Germany), RNA concentration was determined using the Qubit Fluorometric Quantitation and RNA Broad-Range Assay (Thermo Fisher Scientific) and RNA Integrity Number RIN using the Fragment Analyzer 5300 and the Fragment Analyzer RNA kit (Agilent Technologies, Santa Clara, USA). For library preparation, mRNA fraction was enriched using polyA capture from 200 ng of total RNA using the NEB Next Poly(A) mRNA Magnetic Isolation Module (New England Biolabs, Frankfurt, Germany). Next, mRNA libraries were prepared using the NEB Next Ultra II Directional RNA Library Prep Kit for Illumina (New England Biolabs) according to the manufacturer's instructions. Library molarity was determined by measuring the library size (approximately 400 bp) using the Fragment Analyzer 5300 and the Fragment Analyzer DNA HS NGS fragment kit (Agilent Technologies, Santa Clara, USA) and the library concentration (>0.5 ng/µl) using Qubit Fluorometric Quantitation and dsDNA High sensitivity assay (Thermo Fisher Scientific). In the first experiment, libraries were denaturated according to the manufacturer's instructions, diluted to 270 pM and sequenced as paired-end 100 bp reads on an Illumina NovaSeq 6000 (Illumina) with a sequencing depth >25 million clusters per sample.

Read quality of RNA-seq data in fastq files was assessed using ngs-bits (v.2020_06) to identify sequencing cycles with low average quality, adaptor contamination, or repetitive sequences from PCR amplification. Raw expression values were available for 55.421 genes in 4 samples. Raw gene expression was filtered by demanding a minimum expression value of 1 cpm (counts per million) in at least 2 samples. Filtered data contained expression values for 17.210 genes. Data analysis was performed using the STRING database[19].

Protein isolation and proteome analyses

For proteome analyses, single cell suspensions were prepared from placentas of pregnant WT and Qa2$^-$ animals at E18.5. Cells were lysed by adding lysis buffer (5% 1M Tris/HCl pH 7,4, 2% 5M NaCl, 1% Triton X 100, 1% PMSF, 4% protease inhibitor cocktail (Sigma-Aldrich, St. Louis, USA)) on ice followed by snap-freezing in liquid nitrogen. Ten micrograms of each sample were digested in solution with trypsin as described in[63]. After desalting using C18 stage tips, extracted peptides were separated on an Easy-nLC 1200 system coupled to a Q Exactive HFX mass spectrometer (Thermo Fisher Scientific) as described in[64] with slight modifications: The peptide mixtures were separated using a 90 minutes segmented gradient from to 10-33-50-90% of HPLC solvent B (80% acetonitrile in 0.1% formic acid) in HPLC solvent A (0.1% formic acid) at a flow rate of 200 nl/min. The 12 most intense precursor ions were sequentially fragmented in each scan cycle using higher energy collisional dissociation (HCD) fragmentation. Acquired MS spectra were processed with MaxQuant software package version 1.6.7.0 with integrated Andromeda search engine. Database search was performed against a target-decoy Mus musculus database obtained from Uniprot, containing 63.686 protein entries and 286 commonly observed contaminants. Peptide, protein and modification site identifications were reported at a false discovery rate (FDR) of 0.01, estimated by the target/decoy approach. The LFQ (Label-Free Quantification) algorithm was enabled, as well as match between runs and LFQ protein intensities were used for relative protein quantification. Data analysis was performed using the STRING v11 database[19]

Immunohistochemistry

The mouse placentas at E18.5 were fixed in 4.5% formaldehyde (Sigma Aldrich) and paraffin embedded (max. 48 hours). The samples were infiltrated with paraffin wax in a tissue processor (Leica, Wetzlar, Germany). 3-5 µm thick sections were cut with a sledge microtome (Leica, Wetzlar, Germany) and stained with hematoxylin-eosin (H&E), Periodic acid-Schiff (PAS) and PAS diastase (Merck GmbH, Darmstadt, Germany). Slides were analysed using an Axioskop 2 plus Zeiss microscope (Zeiss, Oberkochen, Germany) equipped with a Jenoptik ProgRes C10 (Laser Optik System, Jena, Germany) plus camera and software. To quantify the placental phenotype the slides were further evaluated using a histo score with 0 (no aggregates), 1 (intermediate phenotype) and 2 (prominent aggregates) (Supplementary Figure 5).

For analysis of spiral artery remodeling at E10.5, uterine arteries were ligated by dental floss and the uterus was removed, placed on a polystyrene piece and fixed 4.5% formaldehyde (Sigma Aldrich) and paraffin embedded as described in[65]. 3-5 µm thick sections were stained with H&E and the slides were scanned with the Ventana DP200 (Roche, Basel, Switzerland). Placentas from all animals were analyzed at the midsagittal point, given by the presence of the chorioallantoic attachment. The total vessel and luminal areas of the spiral arteries were measured in the central 2/4 of the decidua basalis[65]. The 5 spiral arteries with the largest and roundest lumen in three consecutive sections (50um between sections) were used for analysis and the mean was calculated.

Statistical analysis

Statistical analysis was done using GraphPad Prism 5.0 (GraphPad Software, La Jolla, CA). Data were analyzed for Gaussian distribution using D`Agostino and Pearson omnibus normality test. Unpaired and normally distributed data were analyzed using the unpaired t-test, unpaired and not normally distributed data were evaluated using the Mann-Whitney test. Paired and normally distributed data were analyzed using the paired t-test and paired and not normally distributed data were analyzed using the Wilcoxon matched pairs signed rank test. A p-value <0.05 was considered as statistically significant.

Declarations

AUTHOR CONTRIBUTIONS

All authors were involved in drafting the article or revising it critically for important intellectual content, and all authors approved the final version to be published. S.D., J.S., A.V., I.G.-M., L.Q.-M., N.C., A.M., C.G. and N.K.-G. contributed to the acquisition of data, analysis, and interpretation of data. C.F.P. provided critical feedback on intellectual content. N.K.-G. and C.G. conceived the study and wrote the paper. N.K.-G. and C.G. contributed equally

ACKNOWLEDGEMENTS

This work was supported by research grants of the Ministerium für Wissenschaft, Forschung und Kunst Baden-Württemberg and the European Social Fund and the Deutsche Forschungsgemeinschaft (DFG). We thank Jianhong Cao from Fred Hutchinson Cancer Research Center, Seattle, USA for providing the sHLA-G and Prof. Stefan Stevanovic from the interfaculty institute for cell biology at Tuebingen University for help with the HLA-G tetramerization.

CONFLICT OF INTEREST STATEMENT

The authors have declared that no conflict of interest exists

References

1. Rai R, Regan L. Recurrent miscarriage. *Lancet.* 2006;368(9535):601-611.

2. Slattery MM, Morrison JJ. Preterm delivery. *Lancet.* 2002;360(9344):1489-1497.

3. Rebmann V, da Silva Nardi F, Wagner B, Horn PA. HLA-G as a tolerogenic molecule in transplantation and pregnancy. *Journal of immunology research.* 2014;2014:297073.

4. LeMaoult J, Krawice-Radanne I, Dausset J, Carosella ED. HLA-G1-expressing antigen-presenting cells induce immunosuppressive CD4+ T cells. *Proc Natl Acad Sci U S A.* 2004;101(18):7064-7069.

5. Contini P, Ghio M, Poggi A, et al. Soluble HLA-A,-B,-C and -G molecules induce apoptosis in T and NK CD8+ cells and inhibit cytotoxic T cell activity through CD8 ligation. *Eur J Immunol.* 2003;33(1):125-

134.

6. Riteau B, Rouas-Freiss N, Menier C, Paul P, Dausset J, Carosella ED. HLA-G2, -G3, and -G4 isoforms expressed as nonmature cell surface glycoproteins inhibit NK and antigen-specific CTL cytolysis. *J Immunol.* 2001;166(8):5018-5026.

7. Gonzalez A, Rebmann V, LeMaoult J, Horn PA, Carosella ED, Alegre E. The immunosuppressive molecule HLA-G and its clinical implications. *Crit Rev Clin Lab Sci.* 2012;49(3):63-84.

8. Comiskey M, Goldstein CY, De Fazio SR, Mammolenti M, Newmark JA, Warner CM. Evidence that HLA-G is the functional homolog of mouse Qa-2, the Ped gene product. *Hum Immunol.* 2003;64(11):999-1004.

9. Warner CM, Panda P, Almquist CD, Xu Y. Preferential survival of mice expressing the Qa-2 antigen. *Journal of reproduction and fertility.* 1993;99(1):145-147.

10. Gabrilovich DI. Myeloid-Derived Suppressor Cells. *Cancer Immunol Res.* 2017;5(1):3-8.

11. Youn JI, Nagaraj S, Collazo M, Gabrilovich DI. Subsets of myeloid-derived suppressor cells in tumor-bearing mice. *J Immunol.* 2008;181(8):5791-5802.

12. Pawelec G, Verschoor CP, Ostrand-Rosenberg S. Myeloid-Derived Suppressor Cells: Not Only in Tumor Immunity. *Frontiers in immunology.* 2019;10:1099.

13. Kostlin N, Hofstadter K, Ostermeir AL, et al. Granulocytic Myeloid-Derived Suppressor Cells Accumulate in Human Placenta and Polarize toward a Th2 Phenotype. *J Immunol.* 2016;196(3):1132-1145.

14. Kostlin N, Kugel H, Spring B, et al. Granulocytic myeloid derived suppressor cells expand in human pregnancy and modulate T-cell responses. *Eur J Immunol.* 2014;44(9):2582-2591.

15. Kostlin-Gille N, Dietz S, Schwarz J, et al. HIF-1alpha-Deficiency in Myeloid Cells Leads to a Disturbed Accumulation of Myeloid Derived Suppressor Cells (MDSC) During Pregnancy and to an Increased Abortion Rate in Mice. *Frontiers in immunology.* 2019;10:161.

16. Ostrand-Rosenberg S, Sinha P, Figley C, et al. Frontline Science: Myeloid-derived suppressor cells (MDSCs) facilitate maternal-fetal tolerance in mice. *J Leukoc Biol.* 2017;101(5):1091-1101.

17. Pan T, Liu Y, Zhong LM, et al. Myeloid-derived suppressor cells are essential for maintaining feto-maternal immunotolerance via STAT3 signaling in mice. *J Leukoc Biol.* 2016.

18. Kostlin N, Ostermeir AL, Spring B, et al. HLA-G promotes myeloid-derived suppressor cell accumulation and suppressive activity during human pregnancy through engagement of the receptor ILT4. *Eur J Immunol.* 2017;47(2):374-384.

19. Szklarczyk D, Gable AL, Lyon D, et al. STRING v11: protein-protein association networks with increased coverage, supporting functional discovery in genome-wide experimental datasets. *Nucleic Acids Res.* 2019;47(D1):D607-D613.

20. Lynge Nilsson L, Djurisic S, Hviid TV. Controlling the Immunological Crosstalk during Conception and Pregnancy: HLA-G in Reproduction. *Frontiers in immunology.* 2014;5:198.

21. Kang X, Zhang X, Liu Z, et al. Granulocytic myeloid-derived suppressor cells maintain feto-maternal tolerance by inducing Foxp3 expression in CD4+CD25-T cells by activation of the TGF-beta/beta-catenin pathway. *Mol Hum Reprod.* 2016;22(7):499-511.

22. Kostlin N, Vogelmann M, Spring B, et al. Granulocytic myeloid-derived suppressor cells from human cord blood modulate T-helper cell response towards an anti-inflammatory phenotype. *Immunology.* 2017;152(1):89-101.

23. Byers SL, Wiles MV, Dunn SL, Taft RA. Mouse estrous cycle identification tool and images. *PLoS One.* 2012;7(4):e35538.

24. Garziera M, Scarabel L, Toffoli G. Hypoxic Modulation of HLA-G Expression through the Metabolic Sensor HIF-1 in Human Cancer Cells. *Journal of immunology research.* 2017;2017:4587520.

25. Yaghi L, Poras I, Simoes RT, et al. Hypoxia inducible factor-1 mediates the expression of the immune checkpoint HLA-G in glioma cells through hypoxia response element located in exon 2. *Oncotarget.* 2016;7(39):63690-63707.

26. Goldman-Wohl DS, Ariel I, Greenfield C, et al. Lack of human leukocyte antigen-G expression in extravillous trophoblasts is associated with pre-eclampsia. *Mol Hum Reprod.* 2000;6(1):88-95.

27. Steinborn A, Varkonyi T, Scharf A, Bahlmann F, Klee A, Sohn C. Early detection of decreased soluble HLA-G levels in the maternal circulation predicts the occurrence of preeclampsia and intrauterine growth retardation during further course of pregnancy. *Am J Reprod Immunol.* 2007;57(4):277-286.

28. Yie SM, Li LH, Li YM, Librach C. HLA-G protein concentrations in maternal serum and placental tissue are decreased in preeclampsia. *Am J Obstet Gynecol.* 2004;191(2):525-529.

29. Watkins A, Wilkins A, Osmond C, et al. The influence of mouse Ped gene expression on postnatal development. *The Journal of physiology.* 2006;571(Pt 1):211-220.

30. McElhinny AS, Exley GE, Warner CM. Painting Qa-2 onto Ped slow preimplantation embryos increases the rate of cleavage. *Am J Reprod Immunol.* 2000;44(1):52-58.

31. Ridder A, Giorgione V, Khalil A, Thilaganathan B. Preeclampsia: The Relationship between Uterine Artery Blood Flow and Trophoblast Function. *Int J Mol Sci.* 2019;20(13).

32. Cui Y, Wang W, Dong N, et al. Role of corin in trophoblast invasion and uterine spiral artery remodelling in pregnancy. *Nature.* 2012;484(7393):246-250.

33. Buhimschi IA, Nayeri UA, Zhao G, et al. Protein misfolding, congophilia, oligomerization, and defective amyloid processing in preeclampsia. *Science translational medicine.* 2014;6(245):245ra292.

34. Cater JH, Kumita JR, Zeineddine Abdallah R, et al. Human pregnancy zone protein stabilizes misfolded proteins including preeclampsia- and Alzheimer's-associated amyloid beta peptide. *Proc Natl Acad Sci U S A.* 2019;116(13):6101-6110.

35. Tong M, Cheng SB, Chen Q, et al. Aggregated transthyretin is specifically packaged into placental nano-vesicles in preeclampsia. *Scientific reports.* 2017;7(1):6694.

36. Sulistyowati S, Bachnas MA, Anggraini ND, et al. Recombinant vascular endothelial growth factor 121 injection for the prevention of fetal growth restriction in a preeclampsia mouse model. *J Perinat Med.* 2017;45(2):245-251.

37. Kostlin-Gille N, Gille C. Myeloid-Derived Suppressor Cells in Pregnancy and the Neonatal Period. *Frontiers in immunology.* 2020;11:584712.

38. Ribechini E, Leenen PJ, Lutz MB. Gr-1 antibody induces STAT signaling, macrophage marker expression and abrogation of myeloid-derived suppressor cell activity in BM cells. *Eur J Immunol.* 2009;39(12):3538-3551.

39. Du M, Yu N, Ding Q, et al. Elevated percentage of CD3(+)T cells and pregnancy outcome in women with recurrent pregnancy loss. *Clin Chim Acta.* 2018;486:341-346.

40. Arenas-Hernandez M, Romero R, Xu Y, et al. Effector and Activated T Cells Induce Preterm Labor and Birth That Is Prevented by Treatment with Progesterone. *J Immunol.* 2019;202(9):2585-2608.

41. Luppi P, Tse H, Lain KY, Markovic N, Piganelli JD, DeLoia JA. Preeclampsia activates circulating immune cells with engagement of the NF-kappaB pathway. *Am J Reprod Immunol.* 2006;56(2):135-144.

42. Hanson EM, Clements VK, Sinha P, Ilkovitch D, Ostrand-Rosenberg S. Myeloid-derived suppressor cells down-regulate L-selectin expression on CD4+ and CD8+ T cells. *J Immunol.* 2009;183(2):937-944.

43. Hosseini A, Dolati S, Hashemi V, Abdollahpour-Alitappeh M, Yousefi M. Regulatory T and T helper 17 cells: Their roles in preeclampsia. *J Cell Physiol.* 2018;233(9):6561-6573.

44. Aluvihare VR, Kallikourdis M, Betz AG. Regulatory T cells mediate maternal tolerance to the fetus. *Nat Immunol.* 2004;5(3):266-271.

45. Zenclussen AC, Gerlof K, Zenclussen ML, et al. Abnormal T-cell reactivity against paternal antigens in spontaneous abortion: adoptive transfer of pregnancy-induced CD4+CD25+ T regulatory cells prevents

fetal rejection in a murine abortion model. *Am J Pathol.* 2005;166(3):811-822.

46. Haist M, Stege H, Grabbe S, Bros M. The Functional Crosstalk between Myeloid-Derived Suppressor Cells and Regulatory T Cells within the Immunosuppressive Tumor Microenvironment. *Cancers (Basel).* 2021;13(2).

47. Kang X, Zhang X, Liu Z, et al. Granulocytic myeloid-derived suppressor cells maintain feto-maternal tolerance by inducing Foxp3 expression in CD4+CD25-T cells by activation of the TGF-beta/beta-catenin pathway. *Mol Hum Reprod.* 2016.

48. Dietz S, Schwarz J, Ruhle J, et al. Extracellular vesicles released by myeloid-derived suppressor cells from pregnant women modulate adaptive immune responses. *Cell Immunol.* 2021;361:104276.

49. Selmani Z, Naji A, Zidi I, et al. Human leukocyte antigen-G5 secretion by human mesenchymal stem cells is required to suppress T lymphocyte and natural killer function and to induce CD4+CD25highFOXP3+ regulatory T cells. *Stem Cells.* 2008;26(1):212-222.

50. Polanczyk MJ, Carson BD, Subramanian S, et al. Cutting edge: estrogen drives expansion of the CD4+CD25+ regulatory T cell compartment. *J Immunol.* 2004;173(4):2227-2230.

51. Wang C, Dehghani B, Li Y, Kaler LJ, Vandenbark AA, Offner H. Oestrogen modulates experimental autoimmune encephalomyelitis and interleukin-17 production via programmed death 1. *Immunology.* 2009;126(3):329-335.

52. Kozasa K, Mabuchi S, Matsumoto Y, et al. Estrogen stimulates female cancer progression by inducing myeloid-derived suppressive cells: investigations on pregnant and non-pregnant experimental models. *Oncotarget.* 2019;10(20):1887-1902.

53. Ozerova M, Nefedova Y. Estrogen promotes multiple myeloma through enhancing the immunosuppressive activity of MDSC. *Leukemia & lymphoma.* 2019;60(6):1557-1562.

54. Yang J, AlTahan A, Jones DT, et al. Estrogen receptor-alpha directly regulates the hypoxia-inducible factor 1 pathway associated with antiestrogen response in breast cancer. *Proc Natl Acad Sci U S A.* 2015;112(49):15172-15177.

55. Favier B, HoWangYin KY, Wu J, et al. Tolerogenic function of dimeric forms of HLA-G recombinant proteins: a comparative study in vivo. *PLoS One.* 2011;6(7):e21011.

56. Liang S, Baibakov B, Horuzsko A. HLA-G inhibits the functions of murine dendritic cells via the PIR-B immune inhibitory receptor. *Eur J Immunol.* 2002;32(9):2418-2426.

57. Kuroki K, Hirose K, Okabe Y, et al. The long-term immunosuppressive effects of disulfide-linked HLA-G dimer in mice with collagen-induced arthritis. *Hum Immunol.* 2013;74(4):433-438.

58. Loumagne L, Baudhuin J, Favier B, Montespan F, Carosella ED, Rouas-Freiss N. In vivo evidence that secretion of HLA-G by immunogenic tumor cells allows their evasion from immunosurveillance. *Int J Cancer.* 2014;135(9):2107-2117.

59. Agaugue S, Carosella ED, Rouas-Freiss N. Role of HLA-G in tumor escape through expansion of myeloid-derived suppressor cells and cytokinic balance in favor of Th2 versus Th1/Th17. *Blood.* 2011;117(26):7021-7031.

60. Zhang W, Liang S, Wu J, Horuzsko A. Human inhibitory receptor immunoglobulin-like transcript 2 amplifies CD11b+Gr1+ myeloid-derived suppressor cells that promote long-term survival of allografts. *Transplantation.* 2008;86(8):1125-1134.

61. Liang BL, Wang ZQ, Cartwright CM, Zhang H, Ding MS, Gillespie WA. Holographic recording with orthogonally polarized beams in a cesium-doped (K0.5Na0.5)0.2(Sr0.75Ba0.25)0.9Nb2O6 crystal. *Appl Opt.* 2001;40(26):4667-4671.

62. Koehn BH, Apostolova P, Haverkamp JM, et al. GVHD-associated, inflammasome-mediated loss of function in adoptively transferred myeloid-derived suppressor cells. *Blood.* 2015;126(13):1621-1628.

63. Borchert N, Dieterich C, Krug K, et al. Proteogenomics of Pristionchus pacificus reveals distinct proteome structure of nematode models. *Genome Res.* 2010;20(6):837-846.

64. Kliza K, Taumer C, Pinzuti I, et al. Internally tagged ubiquitin: a tool to identify linear polyubiquitin-modified proteins by mass spectrometry. *Nat Methods.* 2017;14(5):504-512.

65. Kieckbusch J, Gaynor LM, Colucci F. Assessment of Maternal Vascular Remodeling During Pregnancy in the Mouse Uterus. *J Vis Exp.* 2015(106):e53534.

Figures

Figure 1

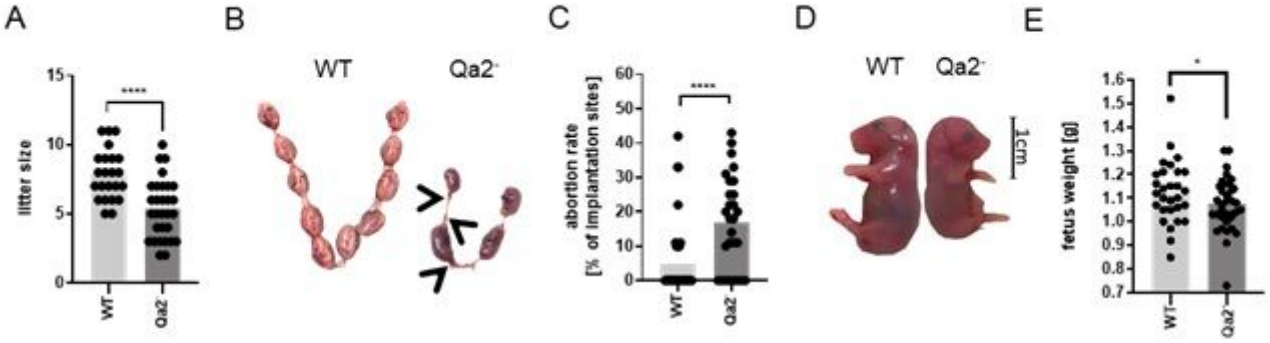

Figure 1

Increased abortion rate in Qa-2- mice Wildtype (WT) and Qa-2 deficient mice (Qa2-) were term-bred and the day when a vaginal plug was detected was defined as day E0.5. Mice delivered spontaneously and litter size was determined or mice were euthanized at E18.5 and uteri containing feto-placental units were removed and inspected. Total implantation sides and resorbing units were counted and fetuses were weighed. (A) Litter size of WT (n=23) and Qa2- mice(n=30). (B) Representative uteri containing feto placental units from WT and Qa2- mice at gestational day E18.5. Arrows show resorbing units. (C) Abortion rate (percentage of resorbed fetuses per litter) of WT (n=39) and Qa2- mice (n=28) at E18.5. (D) Representative WT and Qa2- fetuses at E18.5. (E) Weight of WT (n=29) and Qa2- fetuses (n=35) at E18.5. Each symbol represents an individual animal and the mean is indicated. ****p<0.0001; *p<0.05. Mann-Whitney test (A,C) or unpaired t-test (E).

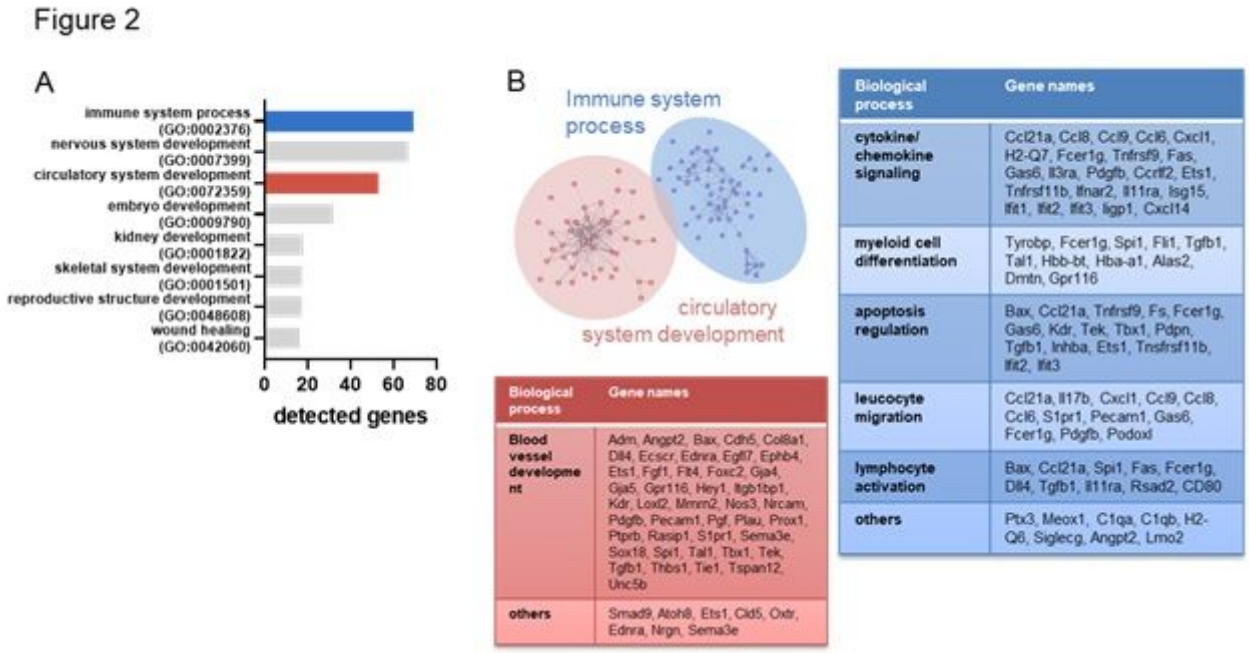

Figure 2

Transcriptome analyses of uteri from wildtype and Qa-2 deficient mice Uteri from wildtype (WT, n=2) and Qa-2 deficient mice (Qa-2-, n=2) were collected at E18.5 of pregnancy and total RNA was isolated and sequenced. (A) Selected biological processes enriched in WT uteri in comparison to Qa2- uteri. (B) Tables of single genes upregulated in WT uteri in comparison to Qa2-uteri assigned to the biological processes “immune system processes” (blue) and “circulatory system development” (red).

Figure 3

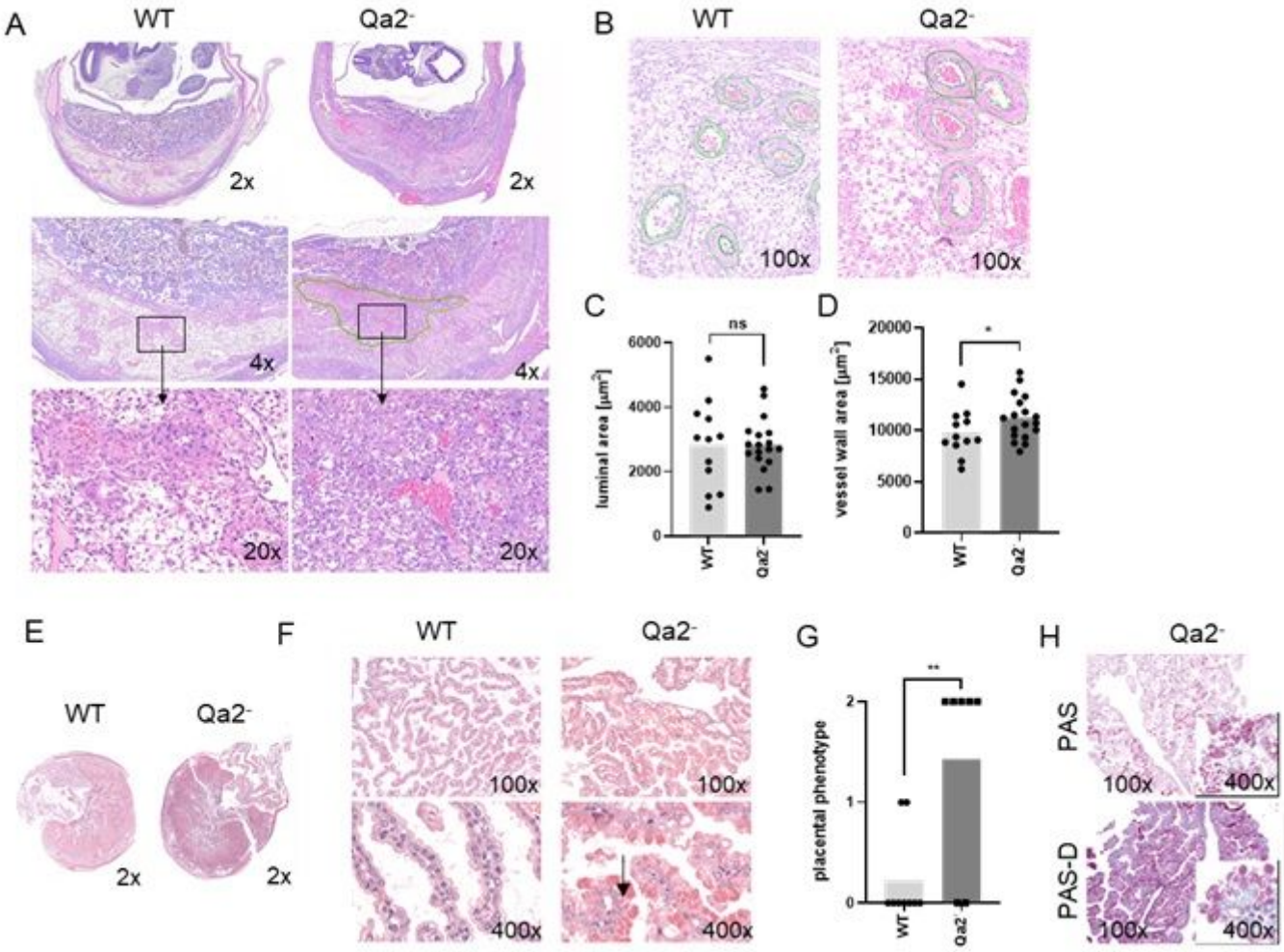

Figure 3

Altered spiral artery remodeling and placental morphology in Qa-2 deficient animals Wildtype (WT) and Qa-2 deficient mice (Qa2-) were term-bred and the day when a vaginal plug was detected was defined as day E0.5. (A-D) Mice were euthanized at E10.5, uterine arteries were ligated and spiral arteries were analyzed. (E-H) Mice were euthanized at E18.5 and placentas were analyzed. (A) Representative images of H&E stained WT and Qa-2- uteri showing cross-section areas of placenta and decidua in different magnifications. The green line shows an area with unorganized trophoblast distribution within the Qa-2- decidua. (B) Representative images of H&E stained WT and Qa-2- uteri showing quantification of spiral artery wall and luminal area. (C) Luminal area of spiral arteries from WT (n=5) and Qa-2- animals (n=5). (D) Vessel wall area of spiral arteries from WT and Qa-2- animals. (E) Representative images of H&E stained cross-section areas of WT and Qa2-placentas. (F) Representative images of H&E stained chorionic villi from WT and Qa2-placentas showing abnormal vacuoles with eosinophilic aggregates in trophoblasts of Qa2-animals (arrow). (G) Grade of eosinophilic aggregation in trophoblasts of WT and Qa2-animals. (H) Representative images of PAS and PAS-diastase stained chorionic villi from a Qa2-placenta showing aggregates still present in PAS-diastase staining. Each symbol represents an individual

measurement (C+D)/animal (G) and the mean is indicated. **p<0.01; *p<0.05; ns = not significant. Unpaired t-test (C+D) or Mann-Whitney test (G).

Figure 4

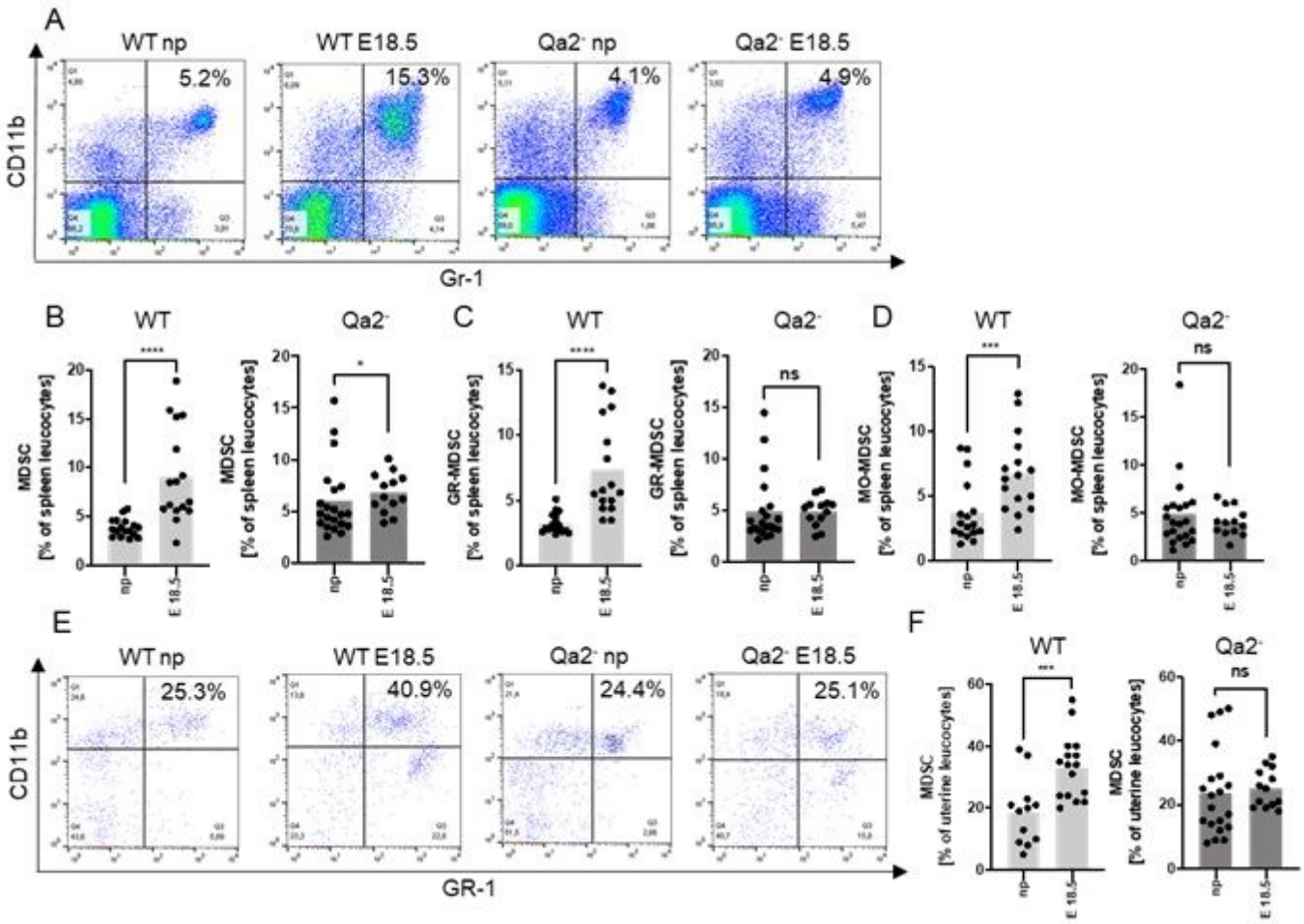

Figure 4

Decreased accumulation of MDSC in Qa-2 deficient mice Wildtype (WT) and Qa-2 deficient mice (Qa2-) were term-bred and the day when a vaginal plug was detected was defined as day E0.5. Mice were euthanized at E18.5 and spleens and uteri were collected. Non-pregnant animals served as controls. Tissues were homogenized and filtered to obtain single cell suspensions and cells were analyzed by flow cytometry. (A) Representative pseudocolor plots for Gr-1 versus CD11b showing the population of MDSC in spleen leucocytes in the upper right quadrant. Cells were pre-gated on CD45. (B-D) Percentages of all MDSC (B), GR-MDSC (C) and MO-MDSC (D) from all spleen leucocytes in non-pregnant animals (np, n=17 for WT and n=21 for Qa-2-) and pregnant animals at E18.5 (n=16 for WT and n=13 for Qa-2-). Light grey graphs represent WT animals and dark grey graphs represent Qa-2- animals. (E) Representative pseudocolor plots for Gr-1 versus CD11b showing the population of MDSC in uterus leucocytes in the upper right quadrant. Cells were pre-gated on CD45. (F) Percentages of MDSC from all uterus leucocytes in non-pregnant animals (np, n=12 for WT and n=20 for Qa-2-) and pregnant animals at E18.5 (n=16 for WT and n=13 for Qa-2-). Light grey graph represents WT animals and dark grey graph represents Qa-2-

animals. Each symbol represents an individual animal and the mean is indicated. ****p<0.0001; ***p<0.001; *p<0.05; ns = not significant. Mann-Whitney test.

Figure 5

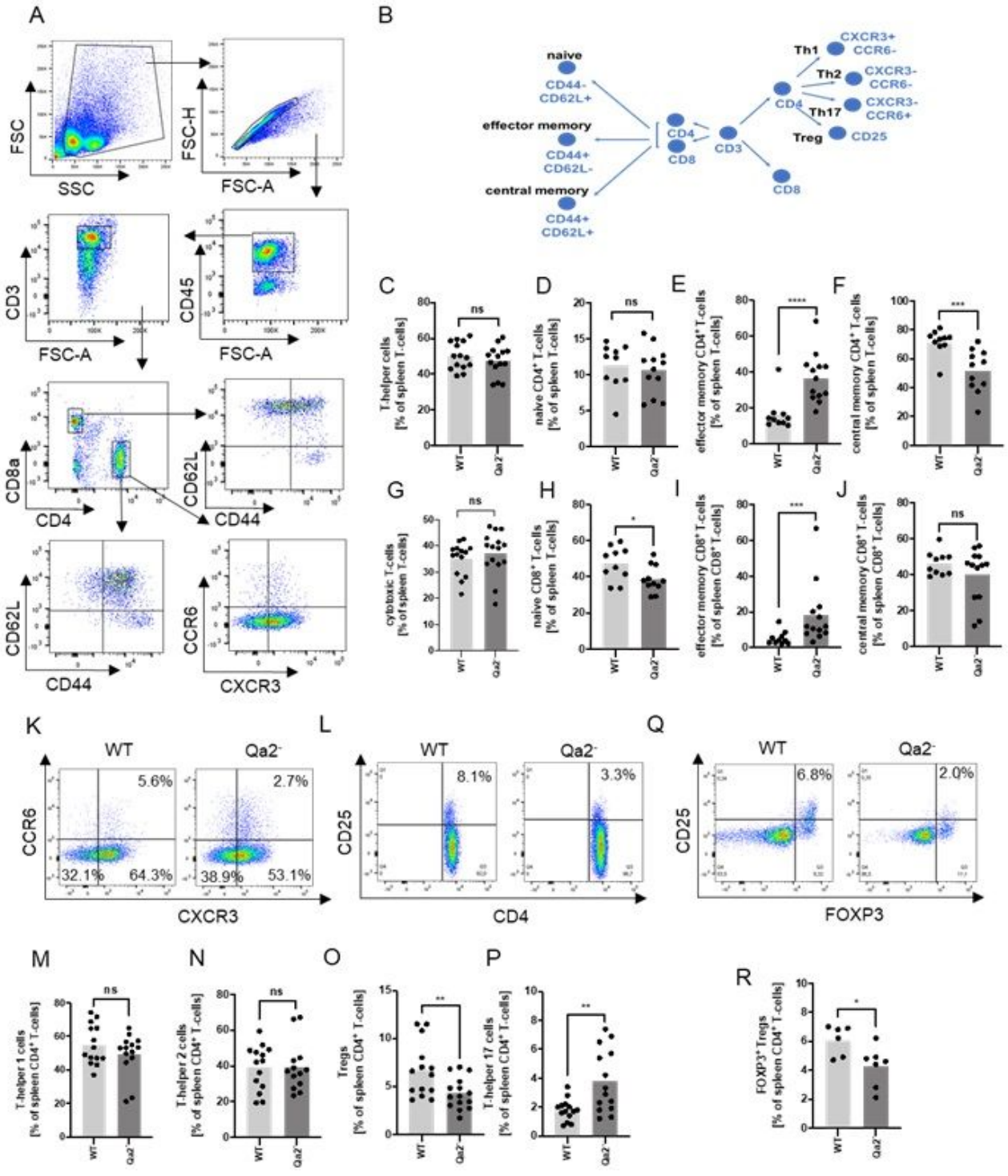

Figure 5

T-cell subpopulations in WT and Qa-2 deficient animals Wildtype (WT) and Qa-2 deficient mice (Qa2-) were term-bred and the day when a vaginal plug was detected was defined as day E0.5. Spleen cells were analyzed by flow cytometry. (A) Gating strategy for gating of T-cell subpopulations. (B) Phenotyping

strategy for T-cell subpopulations. (C-J) Percentages of all T-helper cells (C), naïve T-helper cells (D), effector memory T-helper cells (E), central memory T-helper cells (F), all cytotoxic T-cells (G), naïve cytotoxic T-cells (H), effector memory cytotoxic T-cells (I) and central memory cytotoxic T-cells (J) from all spleen leucocytes in WT (n=10-14) and Qa-2- animals (n=11-15). (K) Representative pseudocolor plots for CXCR3 versus CCR6 showing the populations of T-helper 1 cells (lower right quadrant), T-helper 2 cells (lower left quadrant) and T-helper 17 cells (upper left quadrant) in spleen leucocytes. Cells were pre-gated on CD45, CD3 and CD4. (L) Representative pseudocolor plots for CD4 versus CD25 showing the population of Treg cells in spleen leucocytes in the upper right quadrant. Cells were pre-gated on CD45 and CD3. (M-P) Percentages of all T-helper 1 cells (M), T-helper 2 cells (N), Treg cells (O) and T-helper 17 cells (P) from all spleen leucocytes in WT (n=10-14) and Qa-2- animals (n=11-15). (Q) Representative pseudocolor plots for Foxp3 versus CD25 showing the population of Foxp3+ Treg cells in spleen leucocytes in the upper right quadrant. Cells were pre-gated on CD45, CD3 and CD4. (R) Percentages of Foxp3 Treg cells from all spleen leucocytes in WT (n=6) and Qa-2- animals (n=7). Each symbol represents an individual animal and the mean is indicated. Light grey bars represent WT animals and dark grey bars represent Qa-2- animals. ****p<0.0001; ***p<0.001; **p<0.01; *p<0.05; ns = not signifikant. Mann-Whitney test.

Figure 6

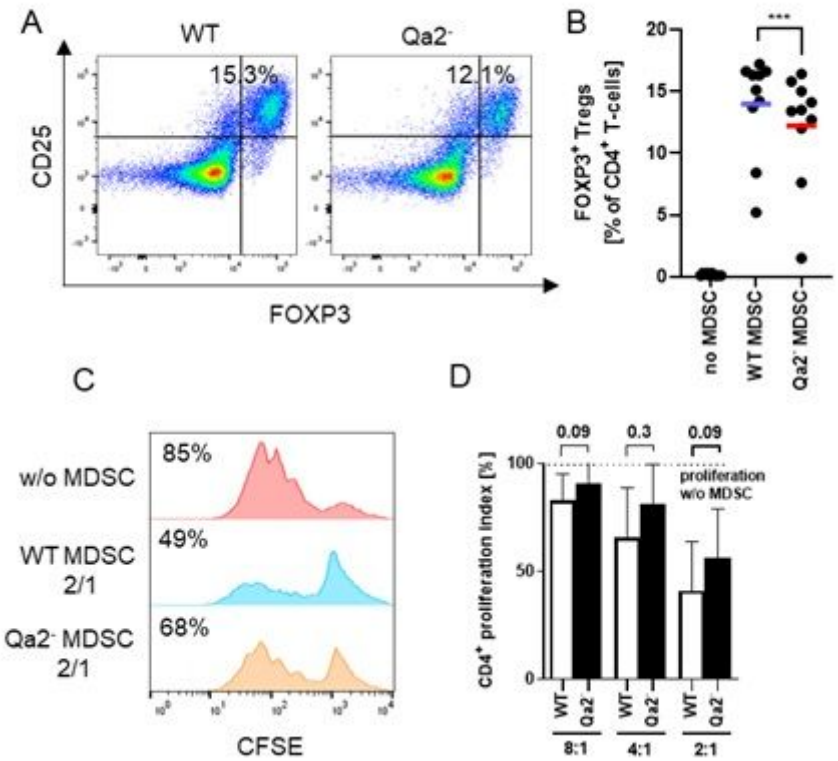

Figure 6

Decreased capacity of Qa-2 deficient MDSC to induce Tregs MDSC were in vitro generated from bone marrow cells (A+B) or isolated by magnetic activated cell sorting from E18.5 pregnant wildtype (WT) and Qa-2 deficient mice (Qa-2-) (C+D) and added to MACS isolated splenic CD4+ T-cells from WT mice. (A)

Representative pseudocolor plots for Foxp3 versus CD25 showing the population of Foxp3+ Treg cells after four days of co-culture with MDSC generated from WT and Qa-2- mice in a 2:1 (T-cells: MDSC) ratio in the upper right quadrant. Cells were pre-gated on CD45, CD3 and CD4. (B) Percentages of Foxp3+ Treg cells of all CD4+ T-cells without addition of MDSC, with addition of MDSC generated from WT mice and with addition of MDSC generated from Qa-2- mice (n=10). (C) Representative histogram plots showing proliferation of CFSE-stained and anti-CD3/CD28 stimulated T-cells without addition of MDSC and with addition of MDSC generated from WT and Qa-2- mice in a 2:1 (T-cells: MDSC) ratio. (D) Inhibitory effect of MDSC from WT mice (white bars) and Qa-2- mice (black bars) on proliferation of CD4+ T-cells in different ratios (T-cells:MDSC) (n=6-7). Dashed line shows proliferation of target CD4+ T-cells without addition of MDSC. Proliferation index was determined as ratio of T-cell proliferation with and without addition of MDSC. Each symbol represents an individual animal and the mean is indicated (A). Bars represent pooled data from 6-7 independent experiments. ***p<0.001; ns = not significant. Wilcoxon matched pairs signed rank test (B) and Mann-Whitney test (D).

Figure 7

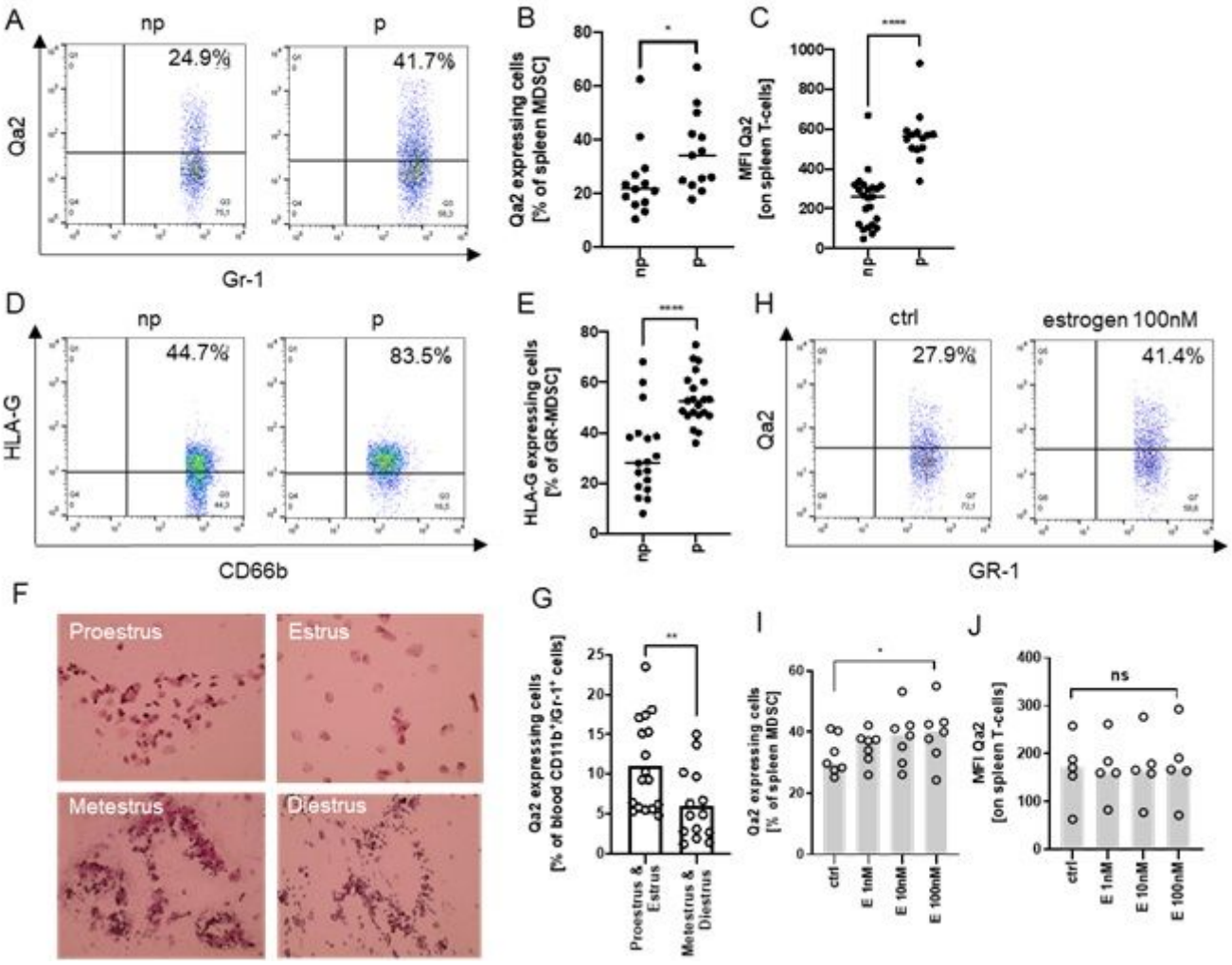

Figure 7

Expression of Qa-2 on MDSC is regulated by estrogen (A) Representative pseudocolor plots for Gr-1 versus Qa-2 from splenocytes from non-pregnant (np) and pregnant (p) wildtype (WT) animals showing

the percentage of Qa-2 expressing MDSC in the upper right quadrant. Cells were pre-gated on CD45 and CD11b. (B) Percentages of Qa-2 expressing MDSC from all spleen MDSC from non-pregnant (n=13) and pregnant WT mice (n=13). (C) MFI for Qa-2 on spleen T-cells from non-pregnant (n=23) and pregnant WT mice (n=14). (D) Representative pseudocolor plots for CD66b versus HLA-G from PBMC from non-pregnant (np) and pregnant (p) women showing the percentage of HLA-G expressing MDSC in the upper right quadrant. (E) Percentages of HLA-G expressing MDSC from all MDSC in the peripheral blood of non-pregnant (n=18) and pregnant women (n=21). (F) Representative images of H&E stained vaginal swabs from the four different phases of the mouse estrus cycle. (G) Percentages of Qa-2 expressing cells from all blood CD11b+/Gr-1+ cells in proestrus & estrus (n=14) and metestrus & diestrus (n=17). (H) Representative pseudocolor plots for Gr-1 versus Qa-2 from splenocytes from WT mice without stimulation (ctrl) and with stimulation with 100nM estrogen showing the percentage of Qa-2 expressing MDSC in the upper right quadrant. Cells were pre-gated on CD45 and CD11b. (I) Percentages of Qa-2 expressing MDSC from all spleen MDSC from WT mice without stimulation and with stimulation with estrogen in rising concentrations (n=7). (J) MFI for Qa-2 on spleen T-cells from wildtype mice without stimulation and with stimulation with estrogen in rising concentrations (n=5). Each symbol represents an individual animal/women and the mean is indicated. ****p<0.0001; **p<0.01; *p<0.05; ns = not significant. Mann-Whitney test (B, C, E, G) and Wilcoxon matched-pairs signed rank test (I-J).

Figure 8

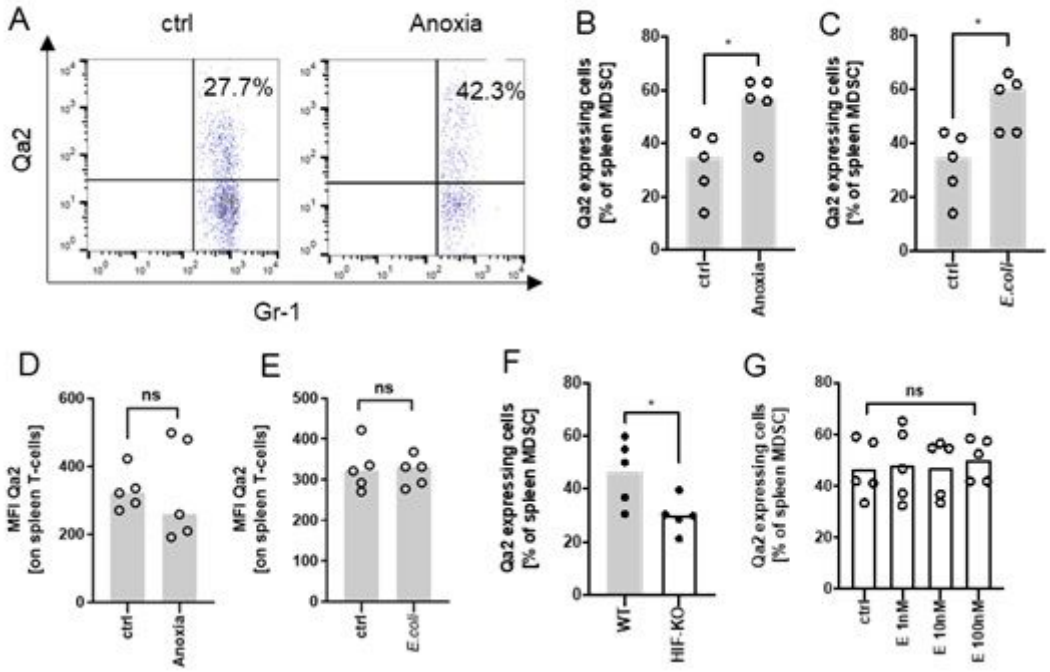

Figure 8

Expression of Qa-2 on MDSC is regulated by HIF-1α (A) Representative pseudocolor plots for Gr-1 versus Qa-2 from splenocytes from wildtype (WT) mice cultured under normoxia (ctrl) or anoxia for 4 h showing the percentage of Qa-2 expressing MDSC in the upper right quadrant. Cells were pre-gated on CD45 and CD11b. (B) Percentages of Qa-2 expressing MDSC from all spleen MDSC from WT mice cultured under

normoxia or anoxia (n=5). (C) Percentages of Qa-2 expressing MDSC from all spleen MDSC from WT mice without stimulation or with stimulation with E. coli (n=5). (D) MFI of Qa-2 on spleen T-cells from WT mice cultured under normoxia or anoxia (n=5). (E) MFI of Qa-2 on spleen T-cells from wildtype mice without stimulation or with stimulation with E. coli (n=5). (F) Percentages of Qa-2 expressing MDSC from all spleen MDSC from WT mice (n=5) and from mice with targeted deletion of HIF-1α in myeloid cells (HIF-KO, n=5). Percentages of Qa-2 expressing MDSC from all spleen MDSC from HIF-KO mice without stimulation and with stimulation with estrogen in rising concentrations (n=5). Each symbol represents an individual animal and the mean is indicated. *p<0.05; ns=not significant. Mann-Whitney test.

Figure 9

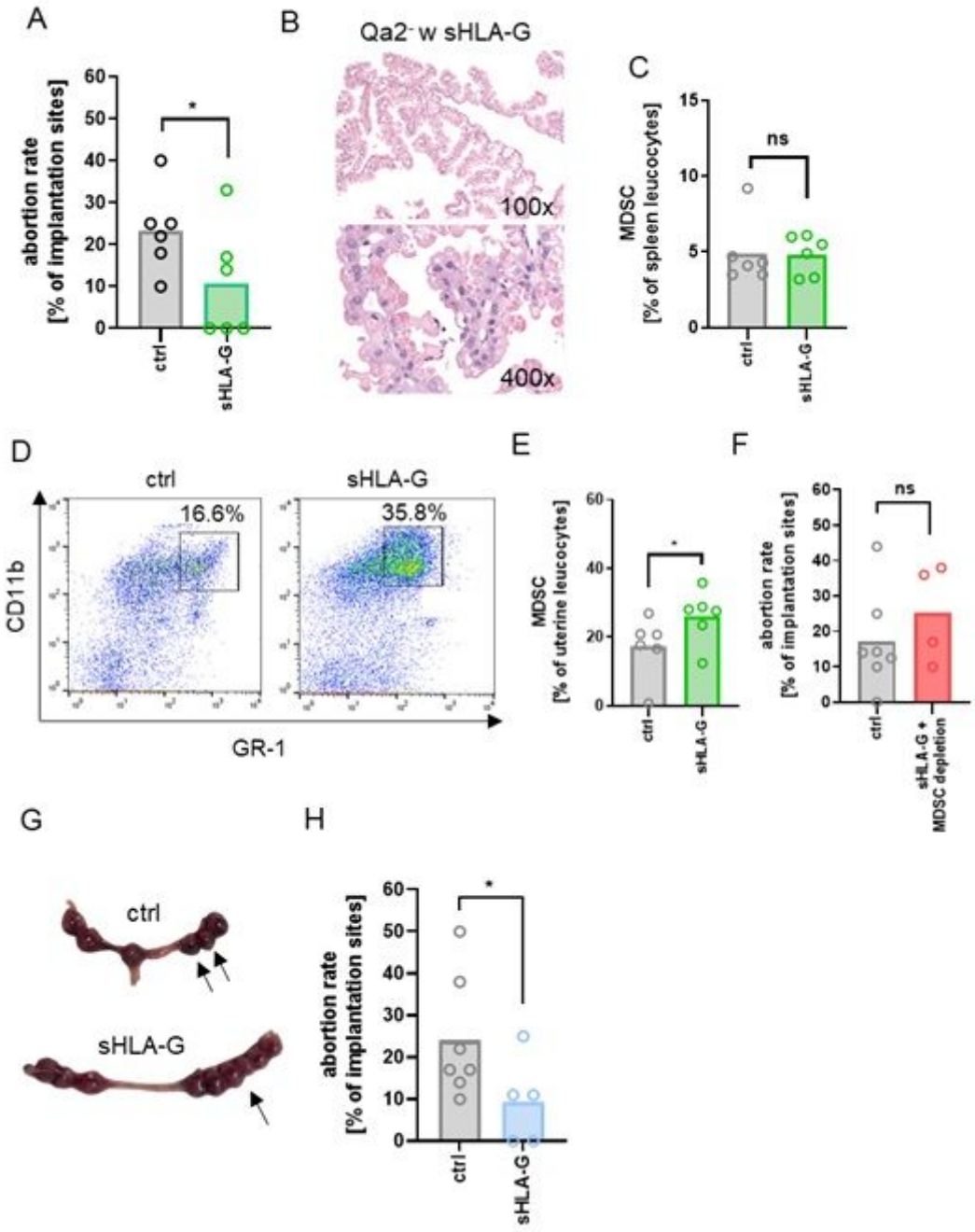

Figure 9

sHLA-G protects from abortions (A-F) Qa-2 deficient mice (Qa2-) were term-bred and the day when a vaginal plug was detected was defined as day E0.5. At E10.5 and E14.5 mice received either PBS, 1µg/g bodyweight sHLA-G or 1µg/g bodyweight sHLA-G and anti-Ly6G-antibody. (A) Abortion rate (percentage of resorbed fetuses per litter) of Qa2- mice after application of PBS (ctrl, n=6) or sHLA-G (n=6) at E18.5. (B) Representative images of H&E stained chorionic villi Qa2- animals that received sHLA-G. (C) Percentages of MDSC in spleens of pregnant Qa2- animals after application of PBS (ctrl, n=6) or sHLA-G (n=6) at E18.5. (D) Representative pseudocolor plots for Gr-1 versus CD11b showing the population of MDSC in uterus leucocytes of Qa2-mice after application of PBS or sHLA-G in the upper right quadrant. Cells were pre-gated on CD45. (E) Percentages of MDSC in uteri of pregnant Qa2- animals after application of PBS (ctrl, n=6) or sHLA-G (n=6) at E18.5. (F) Abortion rate of Qa-2 deficient mice after application of PBS (ctrl, n=7) or sHLA-G and anti-Ly6G-antibody (n=4) at E18.5. (G+H) Female CBA/J mice were term-bred with male DBA/2J mice and the day when a vaginal plug was detected was defined as day E0.5. At E0.5, E3.5, E6.5 and E9.5 mice received either PBS or 1µg/g bodyweight sHLA-G. (G) Representative uteri containing fetal-placental units from PBS (ctrl, n=7) and sHLA-G treated mice (n=5) at gestational day E10.5. Arrows show resorbed fetuses. (H) Abortion rate of CBA/J mice after application of PBS (ctrl, n=7) or sHLA-G (n=5) at E10.5. Each symbol represents an individual animal and the mean is indicated. *p<0.05; ns=not significant. Mann-Whitney test.

Supplementary Files

This is a list of supplementary files associated with this preprint. Click to download.

- SupplementaryFiguresQa2pregnancyfinal.pptx